Intrinsic properties affecting the catalytic activity toward ORR of nanostructured transition metal nitrides as catalysts for hybrid Na-air batteries

Da Zhang , Kaiwen Zhang , Zhipeng Xie , Bowen Xu , Minjie Hou , Yong Lei , Takayuki Watanabe , Bin Yang , Feng Liang *

Posted Date: 16 August 2023

doi: 10.20944/preprints202308.1203.v1

Keywords: transition metal nitride; DC arc plasma; ORR; HSABs; intrinsic property

Article

Efficient Route to Synthesize Transition Metal Nitrides Nanoparticle by Arc Discharge

Da Zhang [1,2,3], Zhipeng Xie [1,2,3], Bin Yang [1,2,3], Yong Lei [4], Takayuki Watanabe [5] and Feng Liang [1,2,3]*

[1] Key Laboratory for Nonferrous Vacuum Metallurgy of Yunnan Province, Kunming University of Science and Technology, Kunming, 650093, China
[2] National Engineering Research Center of Vacuum Metallurgy, Kunming University of Science and Technology, Kunming, 650093, China
[3] Faculty of Metallurgical and Energy Engineering, Kunming University of Science and Technology, Kunming, 650093, China
[4] Institute of Physics & IMN MacroNano® (ZIK), Technical University of Ilmenau, Ilmenau 98693, Germany
[5] Department of Chemical Engineering, Kyushu University, Fukuoka 819-0395, Japan
* Correspondence: whom all correspondence should be addressed. Xuefu Road 253, Kunming, Yunnan Province, P.R. China, 650093. Email: liangfeng@kust.edu.cn (Prof. Liang) Tel & Fax: +86-871-6510720

Abstract: Transition metal nitrides (TMNs) nanoparticles (NPs) often has excellent physical and chemical properties, such as high hardness, wear resistance, a high melting point, superconductivity, excellent magnetic properties, and photoluminescence properties. The efficient and environmentally friendly production of high-purity TMNs NPs, however, remains a significant barrier to the full exploitation of their exceptional qualities. In this paper, an efficient, environmentally friendly, and one-step arc discharge method for preparing high-purity TMNs NPs has been further developed. Furthermore, the influence factors such as gas pressure and current on the morphology and purity of TMNs NPs by arc discharge were investigated. Although as-synthesized TiN, ZrN, and HfN NPs have an oxidation layer thickness of about 0.6, 1.2, and 1.5 nm, respectively, it does not affect the purity of TMNs NPs, which is only inevitable when TMNs NPs with a highly active surface come into contact with the air. Due to the higher energy and more nitrogen atoms and ions that were involved in the formation of metal nitride reactions, the TMNs NPs yield is higher under higher current and gas pressure, but the morphology and purity of TMNs NPs are unaffected. The average size of cubic structural TiN, spherical structural ZrN, and spherical structural HfN is about 81.6, 10.1, and 10.5 nm, respectively. Finally, the economic benefit of the production of TiN, ZrN, and HfN NPs from Ti, Zr, and Hf bulks with 99 % purity was evaluated. The work provides an efficient technique to open up the possibility of technological advancement for preparing efficiently TMNs NPs with high purity and good dispersion.

Keywords: Transition metal nitride nanoparticles; Arc discharge; Efficient production; Influence factor; Production cost

1. Introduction

Transition metal nitrides (TMNs) represented by titanium nitride (TiN), zirconium nitride (ZrN), hafnium nitride (HfN), etc., are a kind of mesenchymal compound because element nitrogen is inserted into transition metal lattices [1]. Due to the insertion of element nitrogen, the expansion of the metal lattice and the increase of the cell constant weaken the interaction force between metal atoms, resulting in the corresponding d-band shrinkage modification and the redistribution of state density near the Fermi level [2]. This modulation gives transition metal nitrides unique physical and chemical properties. Besides, nanosized TMNs have become scientifically and technologically important, in part because of their high surface area and smaller crystallite sizes, which led to changes in the electronic structure, thereby resulting in new interesting optical and electronic properties [3,4]

Researchers have lately been successful in producing TMNs nanoparticles (NPs) utilizing several methods. These approaches can be divided into physical methods, including laser ablation [5], arc discharge [6], and laser plasma sputtering [7], and chemical methods, consisting of direct

 doi:10.20944/preprints202308.1203.v1

nitride of transition metals or transition metal oxides [8], ammonia pyrolysis of transition metal chlorides [9], solvothermal [10], and thermal decomposition of polymer precursors [11]. As to these chemical methods, supreme-quality TMNs NPs could be synthesized when the raw materials are properly chosen, and meanwhile, synthesis processes are easy to control [12]. Nevertheless, the synthesis process usually involves multi-step chemical reactions and requires complicated manipulation, including catalysts, toxic stabilizers, surfactants, or reducing agents in most cases. In addition, in order to improve particle purity and crystallinity, post-treatments consisting of separation, washing, heating, or annealing are required, which are time-consuming and laborious. As a kind of physical method for preparing TMNs NPs, arc discharge synthesis has been proven to be a promising route to efficient production of TMNs NPs because plasma can significantly accelerate reaction rates and even motivate the chemistry that is hardly realized by conventional routes [13,14]. From a practical perspective, arc discharge synthesis offers a low-cost and environmentally friendly alternative and has been demonstrated to be suitable for scaling up NPs throughput. The production rate could linearly scale with reasonable adjustment of synthesis parameters, while the primary particle size remains on the nanoscale [15].

The arc discharge process of synthesizing TMNs NPs is usually optimized by adjusting experimental parameters such as nitrogen pressure and arc current to provide different plasma parameters and spatial distribution, as well as nucleation and growth in the space and time domains. For example, Fu et al. [16] reported that titanium nitride (TiN) NPs were synthesized by direct current (DC) arc discharge under mixed N_2 and Ar at atmospheric pressure and different arc currents. With increasing nitrogen pressure and arc current, the production rate of TiN NPs can be enhanced. Moreover, the crystallite size of TiN NPs increases by almost 20 nm with increasing N_2 pressure, while the increase in arc current has a limited impact on the primary particle size. The reason for the increased productivity may be the enhancement in power input as nitrogen pressure and arc current increase, which causes more material evaporation and in turn leads to an enhancement of the particle production rate. However, Bendavid et al. [17] found that although increasing the arc current would increase the amount of material evaporated, larger TiN NPs were produced at higher arc currents when TiN NPs were synthesized by the arc plasma to elucidate the effect of arc current on TiN NPs production. Besides, Naddaf et al. [18] demonstrated that the average texturing coefficient of (111) orientation and the grain size of both TiN and ZrN increased as N_2 partial pressure increased in arc plasma. Based on the above analysis, N_2 pressure and arc current play a vital role in the synthesis process of TMNs NPs by arc discharge, but the effect mechanism of the two experimental parameters on the formation of TMNs NPs has not been unified, which greatly limits the controlled preparation of TMNs NPs by arc discharge.

Hence, TiN, ZrN, and HfN were environmentally friendly and one-step synthesized by DC arc discharge under different N_2 pressures and currents to elucidate the effect of N_2 pressure and current on TMNs NPs production. The effect of N_2 pressure and current on the formation of TMNs NPs is investigated, and the growth mechanism of TMNs NPs under N_2 pressure and current is achieved. The production rate and cost of TiN, ZrN, and HfN NPs were investigated.

2. Experimental methods

2.1. Preparation of TMNs NPs

The synthesized equipment of TMNs NPs has been introduced in detail in the published study [19]. The diameter and height of a cylindrical DC arc discharge generator are 300 mm. Ti, Zr, and Hf bulks with 99 % purity (Runde Metal Materials Co., Ltd., China) and 10 mm-diameter 99.99% pure tungsten rods (Runde Metal Materials Co., Ltd., China) are served as the cathode and anode, respectively. The tungsten rod is positioned perpendicular to the anodic center and can move towards it to maintain two electrodes 5-10 mm apart since the anode is continuously consumed during the discharge process.

Prior to injecting 50 kPa of 99.99% pure N_2 (Messe, Germany), the chamber pressure is inflated to less than 3 Pa, and the discharge current is kept between 100 and 200 A. To eliminate the effects of

Preprints (www.preprints.org) | NOT PEER-REVIEWED | Posted: 16 August 2023 doi:10.20944/preprints202308.1203.v1

air, the aforementioned procedure is done three times. Initial N_2 with 50-70 kPa pressure as a buffer gas is employed to synthesize TMNs NPs, and the inner wall sediment is collected after the arc discharge.

2.2. Characterization

A transmission electron microscope (TEM, JEM-2100, JEOL, Japan) with an accelerating voltage of 200 kV, a high-resolution transmission electron microscope (HRTEM), and selected area electron diffraction (SAED) are used to study the morphological characteristics, distribution, and particle size of TMNs. X-ray diffraction (XRD, Rigaku D/Max-2500, Rigaku, Japan) measurements with Cu-K radiation in the 2 range of 20 to 80° at the scanning rate of 5 omin-1 are used to characterize the crystalline structure.

3. Results and discussion

Figure 1 shows a schematic diagram of the synthesis process of TMNs NPs by DC arc discharge. In the arc discharge synthesis process, nitrogen molecules are ionized into nitrogen atoms or ions, whereas metal anodes are evaporated into metal atoms due to a high-temperature plasma [20–22]. The evaporated transition metal atoms are promptly chilled, react with the flowing nitrogen atoms or ions by random collisions, and then quickly migrate to a quench area, where the homogeneous nucleation, growth, and coagulation of TMNs NPs occur [23–25]. TMNs NPs are subsequently deposited in the water-cooled chamber.

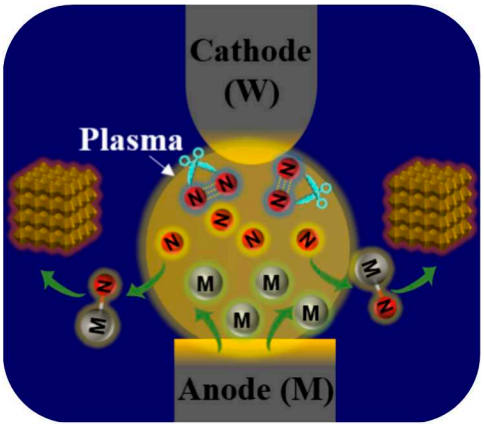

Figure 1. Schematic diagram of synthesis process of TMNs NPs.

To investigate the effect of current and N_2 pressure on the product, a series of experiments on TiN, ZrN, and HfN NPs synthesis at a pressure of 70 kPa N_2 with various currents and at a current of 200 A with various N_2 pressures are carried out, and meanwhile relevant XRD patterns are exhibited in Figure 2, Figure 3, and Figure 4. Obviously, as shown in Figure 2, all XRD patterns show a cubic TiN phase (Joint Committee on Powder Diffraction Standards (JCPDS) card No. TiN 38-1420) and a characteristic peak of TiO (JCPDS card No. TiO 08-0117) in the as-synthesized products [26]. With the rise in N_2 pressure and current, there is no discernible change in the peak intensities of TiN and TiO. According to the process for synthesizing TMNs, the emergence of oxygen in the samples is attributed to the reaction of TiN and oxygen when the sample is exposed to air. This may be the reason for the lack of a remarkable change in the peak intensity of TiN and TiO with increasing N_2 pressure and current. A variety of experiments on ZrN NPs synthesis at 70 kPa N_2 pressures with various currents and at 200 A current with various N_2 pressures are implemented, and relevant XRD patterns are presented in Figure 3. In the as-produced products, all XRD patterns reveal a cubic ZrN phase (JCPDS Card No. ZrN 74-1217), a monoclinic ZrO_2 phase (JCPDS Card No. ZrO_2 37-1484), and a distinctive peak of the $Zr_7O_8N_4$ phase (JCPDS Card No. $Zr_7O_8N_4$ 38-1420) [27,28]. Similar to the synthesis of TiN, the peak intensity of ZrN and $Zr_7O_8N_4$ has also not been noticeably altered with increasing N_2 pressure and current. A sequence of experiments on HfN NPs synthesis at a pressure

Preprints (www.preprints.org) | NOT PEER-REVIEWED | Posted: 16 August 2023 doi:10.20944/preprints202308.1203.v1

of 70 kPa N_2 with various currents and at a current of 200 A with various N_2 pressures are performed, and relevant XRD patterns are illustrated in Figure 4. The surface of the samples synthesized by DC arc discharge using Hf bulk as anode is composed of three phases, including the cubic HfN phase (JCPDS Card No. HfN 33-0592), the HfO_2 phase (JCPDS Card No. HfO_2 34-0104), and the Hf_2ON_2 phase (JCPDS Card No. Hf_2ON_2 50-1171) because HfN NPs have a higher activity in reacting with oxygen than that of TiN and ZrN NPs [29].

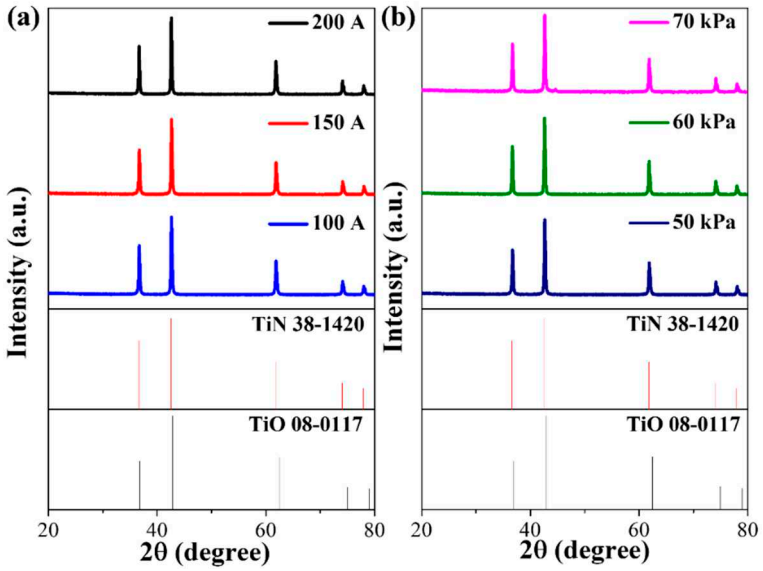

Figure 2. XRD patterns of the samples obtained by DC arc discharge with (a) different currents and (b) different N_2 pressures using Ti bulk as an anode.

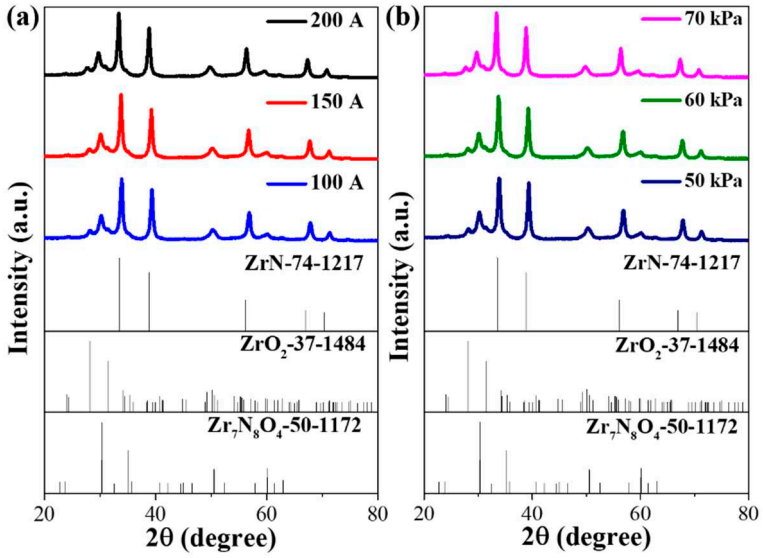

Figure 3. XRD patterns of the samples obtained by arc discharge with (a) different currents and (b) different N_2 pressures using Zr bulk as an anode.

Preprints (www.preprints.org) | NOT PEER-REVIEWED | Posted: 16 August 2023 doi:10.20944/preprints202308.1203.v1

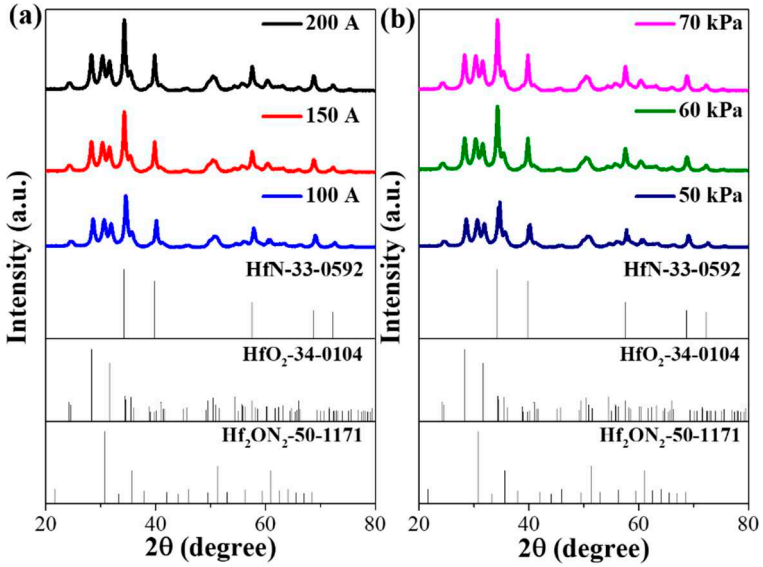

Figure 4. XRD patterns of the samples obtained by the arc discharge with (a) different currents and (b) different N_2 pressures using Hf bulk as an anode.

The differences in anode mass between before and after arc discharge were counted in order to obtain the production rates of TiN, ZrN, and HfN NPs synthesized by the DC arc discharge under various N_2 pressures and currents, as shown in Figure 5. Accordingly, as shown in Figure 5 (a), the production rate of TiN rises progressively with increasing current and N_2 pressure, at 100 A for 0.78 g·min^{-1}, 150 A for 1.31 g·min^{-1}, 200 A for 1.35 g·min^{-1}, 50 kPa for 1.22 g·min^{-1}, and 60 kPa for 1.28 g·min^{-1}, respectively. However, the upward trend of the production rate in synthesizing TiN NPs has slowed down when N_2 pressure is 70 kPa and the current is 200 A. The production rate of ZrN also rises gradually with increasing current and N_2 pressure, at 100 A for 0.84 g·min^{-1}, 150 A for 0.93 g·min^{-1}, 200 A for 1.0 g·min^{-1}, 50 kPa for 0.63 g·min^{-1}, and 60 kPa for 0.9 g·min^{-1}, respectively, as displayed in Figure 5 (b). As displayed in Figure 5 (c), the production rate of HfN also increases gradually with increasing current and N_2 pressure, at 100 A for 0.59 g·min^{-1}, 150 A for 0.92 g·min^{-1}, 200 A for 1.1 g·min^{-1}, 50 kPa for 0.89 g·min^{-1}, and 60 kPa for 1.08 g·min^{-1}, respectively. As a result of increased current and N_2 pressure, both the temperature in the center of the arc and the anodic energy input accelerate the volume evaporation rate of the anode metal. Convective cooling vapor rate, metal vapor supersaturation, and nucleation growth rate all rise with an increase in the vapor density of anodic metal bulk [30]. Hence, the production rate gradually rises as current and N_2 pressures increase.

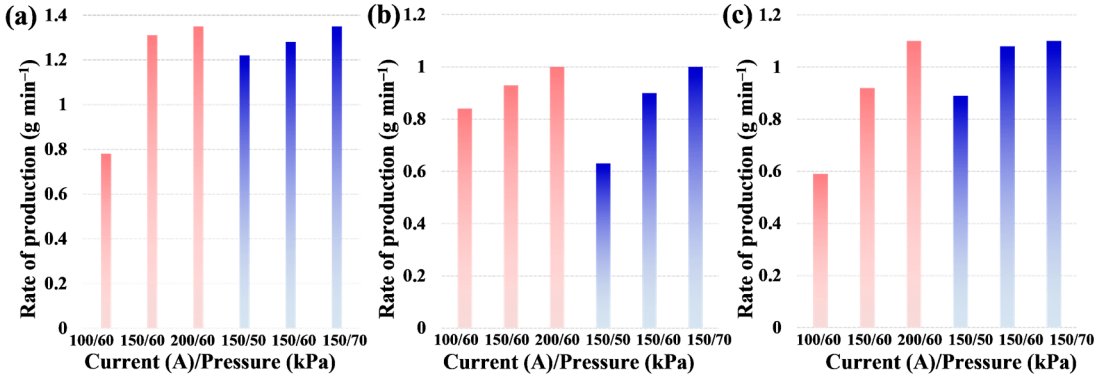

Figure 5. The production rates of (a) TiN, (b) ZrN, and (c) HfN at pressures of 60 kPa N_2 with various currents and at the current of 150 A with various N_2 pressures by the DC arc discharge.

Preprints (www.preprints.org) | NOT PEER-REVIEWED | Posted: 16 August 2023 doi:10.20944/preprints202308.1203.v1

The consequences demonstrate that N_2 pressure and current are closely related to the morphology of the products for the preparation of nanomaterials by DC arc discharge. Therefore, as presented in Figure 6, Figure 7, and Figure 8, the morphology of TiN, ZrN, and HfN synthesized by DC arc discharge under different N_2 pressures and currents is manifested by TEM. Figure 6 shows TEM images of TiN synthesized by DC arc discharge under different N_2 pressures and currents, in which it can be clearly seen that all TiN NPs are regular cubic structures and possess good dispersion. Contrasted with TiN in morphological characteristics, Figure 7 exhibits TEM images of ZrN NPs that have a near-spherical morphology with few intergrowths and a good dispersion. Similar to ZrN in morphological characteristics, Figure 8 (b) shows TEM images of HfN, in which HfN NPs have a near-spherical morphology with few intergrowths and a good dispersion. Remarkably, since the production rate of ZrN and HfN NPs under 70 kPa N_2 pressure with a current of 100 A is extremely low, which can be confirmed by Figure 5, the morphology of samples has not been analyzed. On the basis of the above analysis, the optimum conditions for the preparation of TiN, ZrN, and HfN by DC arc discharge are 200 A current with 70 kPa nitrogen pressure.

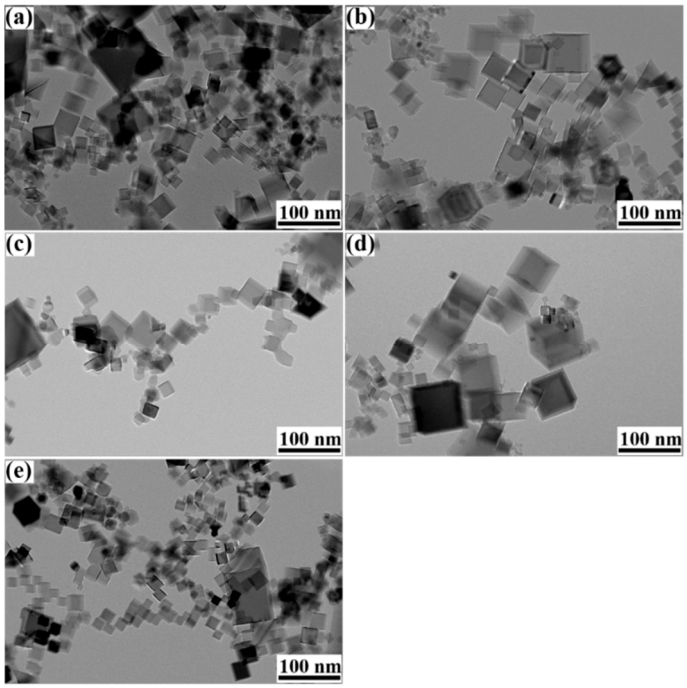

Figure 6. TEM images of TiN prepared under N_2 with various pressures and currents: (a) 100 A-70 kPa, (b) 150 A-70 kPa, (c) 200 A-70 kPa, (d) 50 kPa-200A, (e) 60 kPa-200 A.

Preprints (www.preprints.org) | NOT PEER-REVIEWED | Posted: 16 August 2023 doi:10.20944/preprints202308.1203.v1

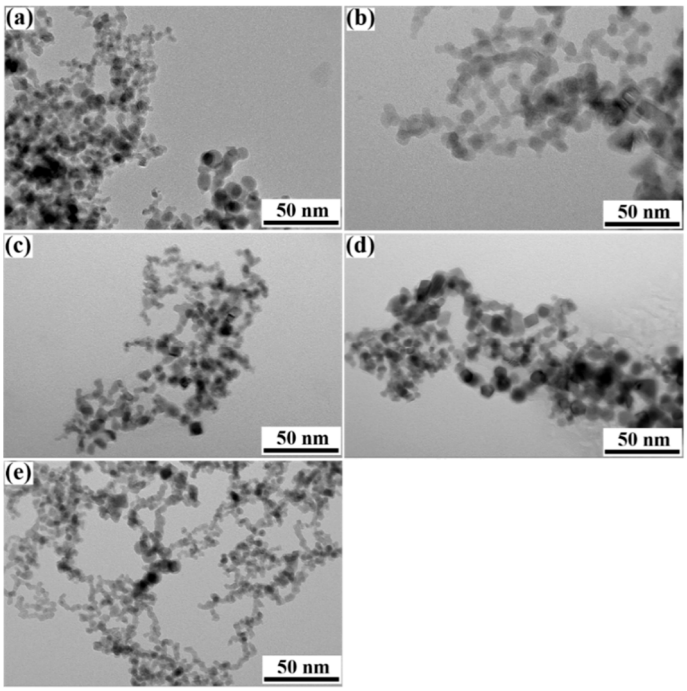

Figure 7. TEM images of ZrN prepared under N_2 with various pressures and currents: (a) 70 kPa-150 A, (b) 70 kPa-200 A, (c) 50 kPa-200 A, (d) 60 kPa-200 A.

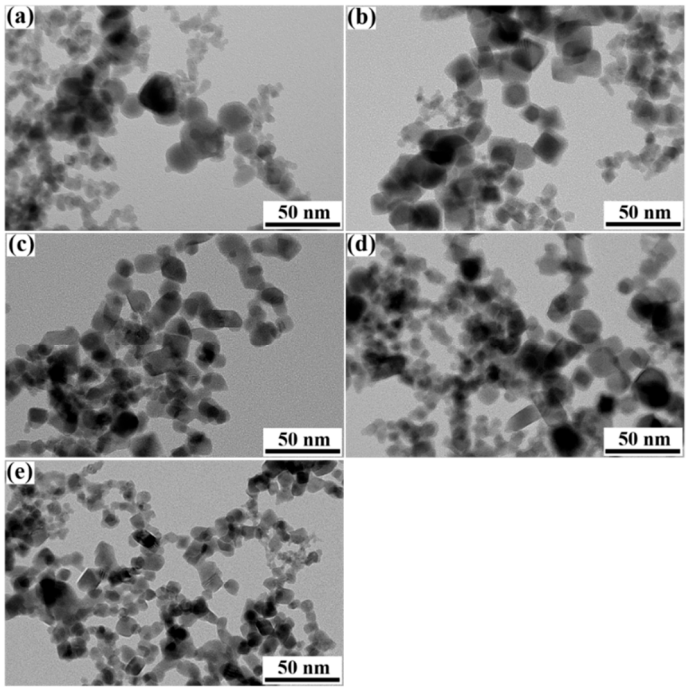

Figure 8. TEM images of HfN prepared under N_2 with various pressures and currents: (a) 70 kPa-150 A, (b) 70 kPa-200 A, (c) 50 kPa-200 A, (d) 60 kPa-200 A.

Figure 9 (a) shows a TEM image of TiN in which it can be clearly seen that all TiN NPs show normal cubic structure, good dispersion, and uniform particle size. Based on the HRTEM image in Figure 9 (b), an initial oxide layer with a thickness of around 0.6 nm on the surface of as-synthesized TiN NPs is generated by the reaction between TiN and air.

The lattice spacing of 0.212 nm, which is in accordance with the lattice fringes of the cubic TiN (200) crystal plane, and the interplanar distance of cubic TiN NPs are shown in Figure 9 (c), suggesting that the as-synthesized TiN has good crystallinity [31]. According to the SAED pattern,

Preprints (www.preprints.org) | NOT PEER-REVIEWED | Posted: 16 August 2023 doi:10.20944/preprints202308.1203.v1

the exposed crystal planes of the as-obtained TiN are (111), (200), (220), and (311) [32,33]. A TEM picture of ZrN is shown in Figure 9(d), which indicates that ZrN NPs have a nearly spherical morphology with few intergrowths and good dispersion. As can be deduced from the HRTEM image of ZrN NPs in Figure 10 (a), the initial oxidation layer of about 1.2 nm thickness on the surface of the as-synthesized ZrN NPs is produced by the reaction between ZrN and air. It is found that the as-synthesized ZrN NPs have the obvious crystal lattices, signifying good crystallinity, and the lattice spacing is 0.264 nm, corresponding to the (111) crystal plane of ZrN [34,35]. According to SAED analysis of ZrN, the exposed crystal planes are (111), (200), (220), and (311), as shown in the inset in Figure 10 (b) [36,37]. A TEM picture of HfN with a nearly spherical shape, few intergrowths, and good dispersion is shown in Figure 10 (c). HRTEM image of HfN in Figure 10 (d) shows the oxidation layer of around 1.5 nm thickness that resulted from the reaction between HfN and air and the obviously crystal lattices. Additionally, HfN NPs exhibit good crystallinity, and the lattice spacing is 0.269 nm, which corresponds to the (111) crystal plane [38,39]. According to the SAED of HfN, as illustrated in the inset of Figure 11 (a), the exposed crystal planes are (111), (200), (220), and (311) [40,41]. Through TEM analysis of more than 200 particles, the size distribution of TiN, ZrN, and HfN NPs is investigated. The size range of TiN in Figure 11 (b) is 40-100 nm, with an average size of 81.6 nm. It can be seen from the size distribution in Figure 11 (c) that the size range of the as-synthesized ZrN NPs has an average size of 10.1 nm and a size range of 5-20 nm. As can be observed from Figure 11 (d), the size range of HfN NPs is 5-20 nm, and the average size is 10.5 nm. In general, all the lattices are perfectly symmetric in cubic microstructure and reveal the (111) crystal plane.

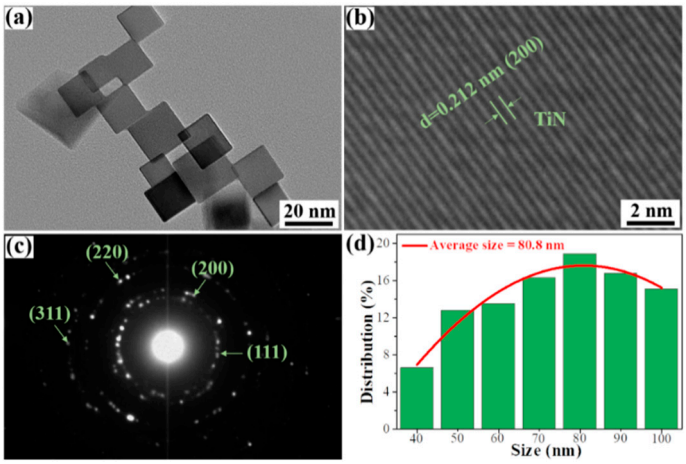

Figure 9. (a) TEM, (b) HRTEM, (c) SAED, and (d) the size distribution images of TiN.

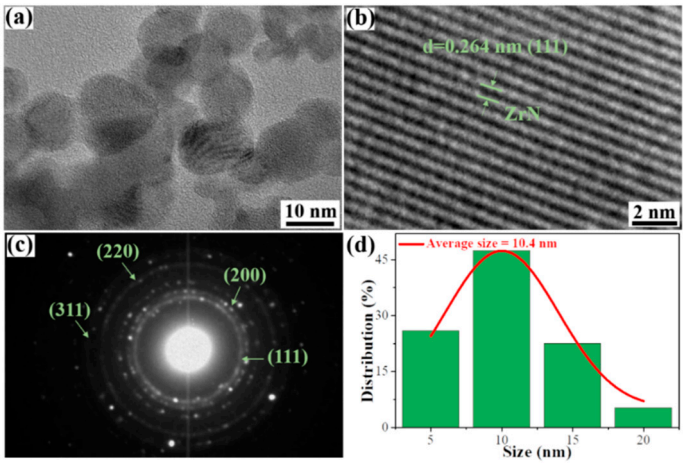

Figure 10. (a) TEM, (b) HRTEM, (c) SAED, and (d) the size distribution images of ZrN.

Preprints (www.preprints.org) | NOT PEER-REVIEWED | Posted: 16 August 2023 doi:10.20944/preprints202308.1203.v1

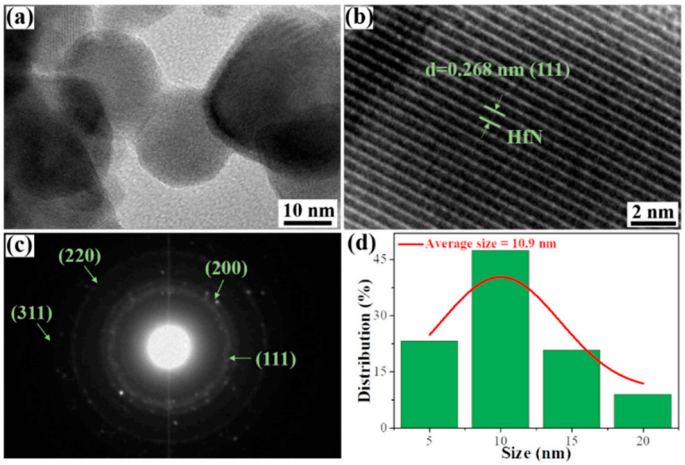

Figure 11. (a) TEM, (b) HRTEM, (c) SAED, and (d) the size distribution images of HfN.

In order to evaluate the economic benefit of the production of TiN, ZrN, and HfN NPs from Ti, Zr, and Hf bulks with 99 % purity in this work, as listed in Table 1, the cost of preparing TiN, ZrN, and HfN NPs by arc discharge is analyzed. Taking 1 kg of the products as an example, according to the above analysis, the cost of producing TiN and ZrN is much lower than that of HfN NPs because the cost of Hf bulk is much higher than that of Ti and Zr bulks. It is evident that utilizing Ti and Zr bulks as the raw material for the production of TiN and ZrN NPs through arc plasma technology not only prepares TMNs NPs in a good environment but also has good economic benefits.

Table 1. The cost of preparation of TiN, ZrN, and HfN NPs.

Samples (1kg)	Cost accounting (¥)				
	Raw Materials	Gas	Electricity	Water	Total
TiN	65	25	12	6	108
ZrN	321	30	16	8	375
HfN	21540	30	16	8	31594

4. Conclusions

In conclusion, TMN NPs, such as TiN, ZrN, and HfN, are efficient, sustainable, and produced in one step by DC arc discharge. Additionally, the effects of gas pressure and current on the morphology and purity of TMNs NPs generated by arc discharge were investigated. Although as-synthesized TiN, ZrN, and HfN NPs have an oxidation layer thickness of about 0.6, 1.2, and 1.5 nm, respectively, it does not affect the purity of TMNs NPs, which is only inevitable when TMNs NPs with a highly active surface come into contact with the air. Due to the higher energy and more nitrogen atoms and ions involved in the formation of metal nitride reactions, the TMNs NPs yield is higher at higher current and gas pressure, but the morphology and purity of TMN NPs are unaffected. According to a series of experiments, the optimum conditions for the preparation of TiN, ZrN, and HfN were determined, which refers to a 200 A current with 70 kPa N_2 pressure. Specifically, the average size of TiN NPs with a regular cubic structure is 81.6 nm. ZrN NPs with a near-spherical structure are 10.1 nm in size on average. The average size of HfN NPs with a near-spherical morphology is 10.5 nm. Finally, the economic benefit of the production of TiN, ZrN, and HfN NPs from Ti, Zr, and Hf bulks with 99 % purity was evaluated. The cost of producing TiN and ZrN NPs is much lower than the production cost of HfN NPs because the cost of Hf bulk is much higher than that of Ti and Zr bulks. The work offers a practical method for producing TMNs NPs with high purity and good dispersion, opening up new avenues for technological development.

Acknowledgments: The work was financially supported by the National Natural Science Foundation of China (12205127, 12175089), the Key Research and Development Program of Yunnan Province (202103AF140006), the Applied Basic Research Programs of Yunnan Provincial Science and Technology Department (202001AW070004,

202301AS070051, 202301AU070064), Yunnan Industrial Innovative Talents Program for "Xingdian Talent Support Plan" (KKXY202252001), Yunnan Program for Introducing Foreign Talents (202305AO350042), and Yunnan Major Scientific and Technological Projects (202202AG050003).

Data availability: The data generated during and/or analyzed during the current study are available from the corresponding author on the reasonable request.

Declarations

Conflicts of Interest: The authors declare no conflict of interest.

References

1. Yu X, Zhou T, Ge J, Wu C. Recent advances on the modulation of electrocatalysts based on transition metal nitrides for the rechargeable Zn-air battery. ACS Mater. Lett. 2020;2(11):1423-1434. https://doi.org/10.1021/acsmaterialslett.0c00339
2. Jamil R, Ali R, Loomba S, Xian J, Yousaf M, Khan K, Shabbir B, McConville C, Mahmood A, Mahmood N. The role of nitrogen in transition-metal nitrides in electrochemical water splitting. Chem Catal. 2021;1(4):802-854. https://doi. org/10.1016/j.checat.2021.06.014
3. Choi D, Kumta P. Synthesis, structure, and electrochemical characterization of nanocrystalline tantalum and tungsten nitrides. J. Am. Ceram. Soc. 2010;90(10):3113-3120. https://doi.org/10.1111/j.1551-2916.2007.01873.x
4. Balogun M, Huang Y, Qiu W, Yang H, Ji H, Tong Y. Updates on the development of nanostructured transition metal nitrides for electrochemical energy storage and water splitting. Mater. Today. 2017;20(8):425-451. https://doi.org/10.1016/j.mattod.2017.03.019
5. Deno H, Kamemoto T, Nemoto S, Koshio A, Kokai F. Formation of TiN-Ir particle films using pulsed-laser deposition and their electrolytic properties in producing hypochlorous acid. Appl. Surf. Sci. 2008;254(9):2776-2782. https://doi.org/10.1016/j.apsusc.2007.10.019
6. Xu S, Xu J, Munroe P, Xie Z. Nanoporosity improves the damage tolerance of nanostructured tantalum nitride coatings. Scr. Mater. 2017;133:86-91. https://doi.org/10.1016/j.scriptamat.2017.02.008
7. Kang J, Park M, Kim J, Park S, Chung D, Yu S, Kim J, Park J, Choi J, Lee K, Jeong J, Ko M, Ahn K, Sung Y. Reactively sputtered nickel nitride as electrocatalytic counter electrode for dye-and quantum dot-sensitized solar cells. Sci. Rep. 2015;5(1):1-11. https://doi.org/10.1038/srep10450
8. Xiang D, Liu Y, Gao S, Tu M. Evolution of phase and microstructure during carbothermal reduction-nitridation synthesis of Ti (C, N). Mater. Charact. 2008;59(3):241-244. https://doi.org/10.1016/j.matchar.2006.12.011
9. Giordano C, Erpen C, Yao W, Antonietti M. Synthesis of Mo and W carbide and nitride nanoparticles via a simple “Urea Glass” route. Nano Lett. 2008;8(12): 4659-4663. https://doi.org/10.1021/nl8018593
10. Chen X, Dye J, Eick H, Elder S, Tsai K. Synthesis of transition-metal nitrides from nanoscale metal particles prepared by homogeneous reduction of metal halides with an alkalide. Chem. Mater. 1997;9(5):1172-1176. https://doi.org/10.1021/cm960565n
11. Choi D, Kumta P. Synthesis, structure, and electrochemical characterization of nanocrystalline tantalum and tungsten nitrides. J. Am. Ceram. Soc. 2010;90(10):3113-3120. https://doi.org/10.1111/j.1551-2916.2007.01873.x
12. Jiang W, Fu Q, Wei H, Yao A. TiN nanoparticles: synthesis and application as near-infrared photothermal agents for cancer therapy. J. Mater. Sci. 2019;54(7):5743-5756. https://doi.org/10.1007/s10853-018-03272-z
13. Kiesler D, Bastuck T, Theissmann R, Kruis F. Plasma synthesis of titanium nitride, carbide and carbonitride nanoparticles by means of reactive anodic arc evaporation from solid titanium. J Nanopart. Res. 2015;17(3):1-13. https://doi.org/10.1007/s11051-015-2967-8
14. Vandenabeele C, Lucas S. Technological challenges and progress in nanomaterials plasma surface modification-a review. Mater. Sci. Eng. R Rep. 2020;139:100521. https://doi.org/10.1016/j.mser.2019.100521
15. Stein M, Kruis F. Scaling-up metal nanoparticle production by transferred arc discharge. Adv Powder Technol. 2018;29(12):3138-3144. https://doi.org/10.1016/j.apt.2018.08.016
16. Fu Q, Kokalj D, Stangier D, Kruis F, Tillmann W. Aerosol synthesis of titanium nitride nanoparticles by direct current arc discharge method. Adv. Powder Technol. 2020;31(9):4119-4128. https://doi.org/10.1016/j.apt.2020.08.012

17. Yick S, Murdock A, Martin P, Kennedy D, Maschmeyer T, Bendavid A. Tuning the plasmonic response of TiN nanoparticles synthesised by the transferred arc plasma technique. Nanoscale. 2018;10(16):7566-7574. https://doi.org/10.1039/C7NR09309H
18. Naddaf M, Abdallah B, Ahmad M, A-Kharroub M. Influence of N_2 partial pressure on structural and microhardness properties of TiN/ZrN multilayers deposited by Ar/N_2 vacuum arc discharge. Nucl. Instrum. Methods Phys. Res. 2016;381:90-95. https://doi.org/10.1016/j.nimb.2016.05.029
19. Zhang D, Ye K, Yao Y, Liang F, Qu T, Ma W, Yang B, Dai Y, Watanabe T. Controllable synthesis of carbon nanomaterials by direct current arc discharge from the inner wall of the chamber. Carbon. 2019;142:278-284. https://doi.org/10.1016/j.carbon.2018.10.062
20. Zhang D, Mylsamy G, Yang X, Xie Z, Su X, Liang F, Yang B, Dai Y. High purity and good dispersity AlN nanoparticles synthesized by an arc discharge with assistance of direct nitridation. Ceram. Int. 2021;47(12):16972-16979. https://doi.org/10.1016/j.ceramint.2021.03.006
21. Duan C, Tanaka M, Kishida M, Watanabe T. Treatment of pyridine in industrial liquid waste by atmospheric DC water plasma. J. Hazard. Mater. 2022;430:128381. https://doi.org/10.1016/j.jhazmat.2022.128381
22. Zhang D, Xie Z, Zhang K, Wang H, Qu T, Ma W, Yang B, Dai Y, Liang F, Lei Y, Watanabe T. Controlled regulation of the transformation of carbon nanomaterials under H_2 mixture atmosphere by arc plasma. Chem. Eng. Sci. 2021; 241:116695. https://doi.org/10.1016/j.ces.2021.116695
23. Cheng Y, Choi S, Watanabe T. Effect of nucleation temperature and heat transfer on synthesis of Ti and Fe boride nanoparticles in RF thermal plasmas. Powder Technol. 2013;246: 210-217. https://doi.org/10.1016/j.powtec.2013.05.028
24. Park Y, Kodama S, Sekiguchi H. Preparation of metal nitride particles using arc discharge in liquid nitrogen. nanomaterials. 2021;11(9):2214. https://doi.org/10.3390/nano11092214
25. Lu Y, Zhang J, Zhao C, Nie M, Wang C, Wang T. Zirconium nitride as a highly efficient nitrogen source to synthesize the metal nitride cluster fullerenes. Sci. China: Chem. 2021;64(1):29-33. https://doi.org/10.1007/s11426-020-9843-2
26. Bang J, Suslick K. Dual templating synthesis of mesoporous titanium nitride microspheres. Adv. Mater. 2009;21(31):3186-3190. https://doi.org/10.1002/adma.200802309
27. Yugeswaran S, Ananthapadmanabhan P, Kumaresan L, Kuberan A, Sivakumar S, Shanmugavelayutham G, Ramachandran K. Synthesis of zirconium nitride from zircon sand by transferred arc plasma assisted carbothermal reduction and nitridation process. Ceram. Int. 2018;44(12):14789-14796. https://doi.org/10.1016/j.ceramint.2018.05.109
28. Lam D, Suematsu H, Ogawa T. Characterization of ZrN, ZrO_2 and β′-$Zr_7O_{11}N_2$ nanoparticles synthesized by pulsed wire discharge. J. Am. Ceram. Soc. 2017;100(10):4884-4892. https://doi.org/10.1111/jace.15012
29. O'Neill D, Frehan S, Zhu K, Zoethout E, Mul G, Garnett E, Huijser A, Askes S. Ultrafast photoinduced heat generation by plasmonic HfN nanoparticles[J]. Adv. Opt. Mater. 2021;2100510. https://doi.org/10.1002/adom.202100510
30. Vandenabeele, Lucas S. Technological challenges and progress in nanomaterials plasma surface modification-A review. Mater. Sci. Eng. R Rep. 2019;139:100521. https://doi.org/10.1016/j.mser.2019.100521
31. Liu M, Dong Y, Wu Y, Feng H, Li J. Titanium nitride nanocrystals on nitrogen-doped graphene as an efficient electrocatalyst for oxygen reduction reaction. Chem. Eur. J. 2013;19(44):14781-14786. https://doi.org/10.1002/chem.201302425
32. Kaneko K, Kitawaki K, Sadayama S, Razavi H, Hernandez-Garrido J, Midgley P, Okuyama H, Uda M, Sakka Y. Fabrication and characterization of TiN nanocomposite powders fabricated by DC arc-plasma method. J. Alloys Compd. 2010;492(1):685-690. https://doi.org/10.1016/j.jallcom.2009.12.017
33. Tavares J, Coulombe S, Meunier J. Synthesis of cubic-structured monocrystalline titanium nitride nanoparticles by means of a dual plasma process. J. Phys. D: Appl. Phys. 2009;42(10):102001. http://iopscience.iop.org/0022-3727/42/10/102001
34. Yuan Y, Wang J, Adimi S, Shen Hangjia, Thomas Tiju, Ma Ruguang, Attfield J, Yang M. Zirconium nitride catalysts surpass platinum for oxygen reduction. Nat. Mater. 2020;19(3):282-286. https://doi.org/10.1038/s41563-019-0535-9
35. Li J Y, Sun Y, Tan Y, Xu F, Shi X, Ren N. Zirconium nitride (ZrN) fibers prepared by carbothermal reduction and nitridation of electrospun PVP/zirconium oxychloride composite fibers. Chem. Eng. J. 2008;144(1):149-152. https://doi.org/10.1016/j.cej.2008.04.037

36. Chen Y, Deng C, Yu C, Ding J, Zhu H. Molten-salt nitridation synthesis of cubic ZrN nanopowders at low temperature via magnesium thermal reduction. Ceram. Int. 2018;44(7):8710-8715. https://doi.org/10.1016/j.ceramint.2018.02.019
37. Reddy R, Kamaraj M, Mudali U, Chakravarthy S, Sarathi R. Generation and characterization of zirconium nitride nanoparticles by wire explosion process. Ceram. Int. 2012;38(7):5507-5512. https://doi.org/10.1016/j.ceramint.2012.03.065
38. Zerr A, Miehe G, Riedel R. Synthesis of cubic zirconium and hafnium nitride having Th3P4 structure. Nat. Mater. 2003;2(3):185-189. https://doi.org/10.1038/nmat836
39. Defilippi C, Shinde D, Dang Z, Manna L, Hardacre C, Greer A, D'Agostino C, Giordano C. HfN nanoparticles: An unexplored catalyst for the electrocatalytic oxygen evolution reaction. Angew. Chem. 2019;58(43):15464-15470. https://doi.org/10.1002/anie.201908758
40. Hu C, Zhang X, Gu Z, Huang H, Zhang S, Fan X, Zhang W, Wei Q, Zheng W. Negative effect of vacancies on cubic symmetry, hardness and conductivity in hafnium nitride films. Scr. Mater. 2015;108:141-146. https://doi.org/10.1016/j.scriptamat.2015.07.002
41. Gu Z, Hu C, Huang H, Zhang S, Fan X, Wang X, Zheng W. Identification and thermodynamic mechanism of the phase transition in hafnium nitride films. Acta Mater. 2015;90:59-68. https://doi.org/10.1016/j.actamat.2015.02.026